J. Math. Biol. (2007) 55:541–573
DOI 10.1007/s00285-007-0094-6

Mathematical Biology

Effects of rapid prey evolution on predator–prey cycles

Laura E. Jones · Stephen P. Ellner

Received: 16 October 2006 / Revised: 15 March 2007 / Published online: 5 May 2007
© Springer-Verlag 2007

Abstract We study the qualitative properties of population cycles in a predator–prey system where genetic variability allows contemporary rapid evolution of the prey. Previous numerical studies have found that prey evolution in response to changing predation risk can have major quantitative and qualitative effects on predator–prey cycles, including: (1) large increases in cycle period, (2) changes in phase relations (so that predator and prey are cycling exactly out of phase, rather than the classical quarter-period phase lag), and (3) "cryptic" cycles in which total prey density remains nearly constant while predator density and prey traits cycle. Here we focus on a chemostat model motivated by our experimental system (Fussmann et al. in Science 290:1358–1360, 2000; Yoshida et al. in Proc roy Soc Lond B 424:303–306, 2003) with algae (prey) and rotifers (predators), in which the prey exhibit rapid evolution in their level of defense against predation. We show that the effects of rapid prey evolution are robust and general, and furthermore that they occur in a specific but biologically relevant region of parameter space: when traits that greatly reduce predation risk are relatively cheap (in terms of reductions in other fitness components), when there is coexistence between the two prey types and the predator, and when the interaction between predators and undefended prey alone would produce cycles. Because defense has been shown to be inexpensive, even cost-free, in a number of systems (Andersson et al. in Curr Opin Microbiol 2:489–493, 1999: Gagneux et al. in Science 312:1944–1946, 2006; Yoshida et al. in Proc Roy Soc Lond B 271:1947–1953, 2004), our discoveries may well be reproduced in other model systems, and in nature. Finally, some of our key results are extended to a general model in which functional forms for the predation rate and prey birth rate are not specified.

L. E. Jones (✉) · S. P. Ellner
Ecology and Evolutionary Biology, Cornell University, Ithaca, NY 14853, USA
e-mail: lej4@cornell.edu

Keywords Predator–prey · Consumer-resource · Cycles · Chemostat · Evolution

Mathematics Subject Classification (2000) 92D25 · 92D40 · 92D15 · 34C15

1 Introduction

Understanding the potential effects of rapid evolution on the dynamics of natural ecosystems is critical to predicting how populations will adapt to a changing environment. Populations in the wild today face unprecedented stress from habitat loss or degradation, harvesting pressure, species introductions and climate change. In addition, otherwise well-intentioned attempts at conservation or management often fail to take into account the potential for rapid evolutionary responses to intervention [25].

It is now well documented, in both natural and experimental settings, that trait evolution can occur on the same time scale as population dynamics [21,23,31,42]. Laboratory systems provide examples where rapid trait evolution in response to population dynamics has been observed directly [10,11,29] or inferred via modeling (e.g., [46,48]). Furthermore, observations of rapid evolution and its consequences in response to a changing natural environment (e.g., [4,13,18,20,22,30,35]) or to anthropogenic changes, such as size-selective fishing mortality [14,30] and hatchery rearing of exploited fish species [22], continue to accumulate. For reviews on this topic see [6,21,37,49].

Prey are under strong selection to avoid predation, because the risk of getting eaten is very strong natural selection. Prey genetic diversity may then allow rapid evolution of resistance to predation, akin to the rapid evolution of microbial pathogens in response to antibiotics. The direct cost of traits conferring defense against predation may have demographic costs to the prey that match or exceed the impact of predation (see [34]; most studies to date involve plastic traits, but the cost for a heritable defensive trait should be similar). For example, the development of armored spines by *Daphnia* exposed to chemicals from fish reduces lifetime fitness by diverting energy from progeny to defense [7]. Thus, by focusing exclusively on changes in population *numbers* without considering changes in the *properties* of the individuals in the population and the associated demographic costs, conventional models of population and community dynamics may give us only half the story.

Our experimental system is a predator–prey microcosm with rotifers, *Brachionus calyciflorus*, and their algal prey, *Chlorella vulgaris*, cultured together in nitrogen-limited, continuous flow-through chemostats. In prior studies we have shown that coexistence of edible and inedible prey genotypes allows the prey to evolve in response to predation pressure at high predator densities, and in response to nutrient limitation at high prey densities. The alternation between selection favoring and disfavoring defensive traits that trade off against efficient nutrient uptake [47] leads to cyclic prey evolution in concert with predator–prey population cycles. Recent work in this system has used PCR techniques to directly track density changes in two algal clones, differing in defense traits, in response to varying predation pressure [29]. Evolution in the prey can lead to "evolutionary" cycling [38,46], where the predator and prey exhibit extended, out-of-phase population cycles (Fig. 1a), or in some circumstances, the odd

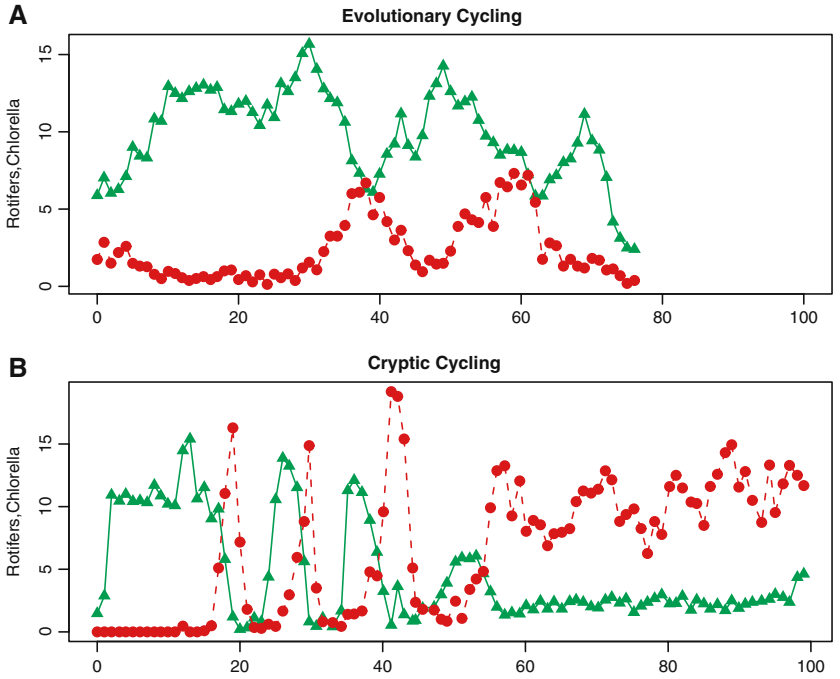

Fig. 1 Example of predator–prey dynamics in experimental rotifer–alga chemostats [15,46]. **a** Evolutionary cycles. *Chlorella* are shown in *solid line*, and the rotifer predator is shown dashed. Prey and predator oscillations are nearly out-of-phase, unlike the quarter-phase shift seen in classic predator–prey cycles. **b** Cryptic cycles. Initially the system exhibits classic predator–prey cycles, which would be expected when a single (edible) prey type is dominant. At about day 55 the system switches to cryptic cycles, which would be expected if a highly defended (inedible) type with low cost for defense arose by mutation. The estimated period of cycles for the predator data on days 59–93 is 16.5 days (estimated using the Lomb periodogram [33]), and the presence of periodicity is significant ($P < 0.001$ using either Fisher's exact test or χ^2 test). A switch from classic to cryptic cycles when a defended type arises by mutation has been documented in bacteria-phage chemostats [11]

phenomenon of "cryptic cycles", where the predator alone exhibits regular population cycles but the prey appear to remain in steady state (Fig. 1b). In cryptic cycling, densities of edible and inedible prey cycle out of phase with each other, driven by changes in predator abundance, in such a way that total prey density remains nearly constant [48]. Evolutionary and cryptic cycles are not unique to this study system: we have observed evolutionary cycles in a chemostat system with rotifers and the flagellated algae *Chlamydomonus*, and cryptic dynamics have been observed in bacteria-phage microcosms [11,48]. We are motivated here by these sorts of perplexing experimental results.

Before conclusions based on laboratory systems or manipulated natural systems are applied to the natural world, we must ask if the conclusions are likely to be robust: are they limited to the special conditions in the experimental systems, or should we expect to see them in a broad range of conditions in nature? This paper is an attempt, using theory, to answer the questions: how general is the phenomenon of evolutionary

cycling in predator–prey systems, under what circumstances might these dynamics be observed, and what are the implications of this type of phenomenon for natural systems? Our results show that evolutionary cycles are indeed a general and robust consequence of rapid prey evolution during predator–prey cycling (Sect. 5), and that cryptic cycles emerge as a limiting case of evolutionary cycles when anti-predator defense is cheap but effective (cf. Sect. 6).

2 The model

Our model is based on an experimental predator–prey microcosm with rotifers, *Brachionus calyciflorus*, and their algal prey, *Chlorella vulgaris*, cultured together in a nitrogen-limited, continuous flow-through chemostat system. This system was first described by Fussmann et al. [15], further characterized by Schertzer et al. [38] and Yoshida et al. [46,47], and equilibrium properties studied by Jones and Ellner [24]. *Brachionus* in the wild are facultatively sexual, but because sexually produced eggs wash out of the chemostat before offspring hatch, our rotifer cultures have evolved to be entirely parthenogenic [16]. The algae also reproduce asexually [32], so evolutionary change in the prey occurs as a result of changes in the relative frequency of different algal clones.

We use a system of ordinary differential equations to describe the population and prey evolutionary dynamics in the experimental microcosms [24,46]. Genetic variability and thus the possibility of evolution in the prey is introduced by explicitly representing the prey population as a finite set of asexually reproducing clones. Each clone is characterized by its palatability p, which represents the conditional probability that an algal cell is digested rather than being ejected alive, once it has been ingested by a predator [29].

The model consists of two equations for the limiting nutrient and rotifers, plus two equations for two prey clones or types. In the following equations, N is nitrogen (μmol/l), C_i represents concentration of the ith algal clone (10^9 cells/l), where $i = 1, 2$. Though the model can accommodate any number of clones, we limit the number to two for reasons discussed below. B is total population density for the predator *Brachionus* (individuals/l). Rotifer mortality in the chemostat is negligibly small (≈ 0.05/days) relative to the washout rate δ, so for the sake of simplicity is omitted here. The parameters χ_c, χ_b are conversions between consumption and recruitment rates (additional model parameters are defined in Table 1).

$$\begin{aligned}
\frac{dN}{dt} &= \delta(N_I - N) - \rho_c \sum_{i=1}^{2} \frac{NC_i}{K_c(p_i) + N} \\
\frac{dC_i}{dt} &= C_i \left[\chi_c \rho_c \frac{N}{K_c(p_i) + N} - \frac{G p_i B}{(K_b + \sum p_i C_i)} - \delta \right] \qquad (1) \\
\frac{dB}{dt} &= B \left[\chi_b \frac{G \sum p_i C_i}{K_b + \sum p_i C_i} - \delta \right]
\end{aligned}$$

Table 1 Parameter estimates for the *Chlorella-Brachionus* microcosm system. Set: adjustable parameters set by the experimenter. TY: Unpublished experimental data (Yoshida et al., in preparation) Fitted: Estimated by numerically optimizing the goodness-of-fit between model output and data on total prey and predator population dynamics from two experiments (originally reported by Fussmann et al. [15]) in which regular cycles occurred

Parameter	Description	Value	Reference
N_I	Limiting nutrient conc. (supplied medium)	80μmol N/l	Set
δ	Chemostat dilution rate	variable (d)	Set
V	Chemostat volume	0.33 l	Set
χ_c	Algal conversion efficiency (10^9 cells/μmol N)	0.05	[15]
χ_b	Rotifer conversion efficiency	$\approx$ 54, 000 rotifers/10^9 algal cells	Fitted
m	Rotifer mortality	0.055/day	[15]
λ	Rotifer senescence rate	0.4/day	[15]
K_c	Minimum algal half-saturation	4.3 μ mol N/l	[15]
K_b	Rotifer half-saturation	0.835×10^9 algal cells/l	TY
β_c	Maximum algal recruitment rate	3.3/day	TY
ω_c	N content in 10^9 algal cells	20.0 μmol	[15]
ϵ_c	Algal assimilation efficiency	1	[15]
G	Rotifer maximum consumption rate	5.0×10^{-5} l/day	TY
α_1	Shape parameter in algal tradeoff	variable, $\alpha_1 > 0$	Fitted
α_2	Scale parameter in algal tradeoff	variable, $\alpha_2 > 0$	Fitted

where

$$F_{C,i}(N) = \rho_c N/(K_c(p_i) + N) \tag{2}$$

and

$$F_b(C_i) = GC_i/(K_b + \sum_{i=1}^{2} p_i C_i) \tag{3}$$

are functional response equations describing algal and rotifer consumption rates, respectively, and where $\rho_c = \omega_c \beta_c/\epsilon_c$.

Equation (2) assumes that there is an instantaneous conversion between nutrient uptake and offspring, and that the yield of offspring per unit of nutrient is constant. Although these assumptions not strictly valid, the dynamic complexities that can occur if these assumptions are violated (e.g., [5,36,45]) have not been observed in our experimental system (e.g., in the absence of predators, algal populations always converge monotonically to a steady state density).

Equation (3) is derived from the predator's clearance rate (the volume of water per unit time that an individual filters to obtain food), assuming that clearance rate is a decreasing function of the total prey food value $\sum_{i=1}^{2} p_i C_i$). That is, lower prey palatability results in the predators increasing their clearance rate, exactly as if prey were less abundant. We also considered a model in which clearance rate depends only on the total prey density, but it could not be fitted as well to our experimental data on population cycles. Elsewhere [29,46] we have used a more complicated expression for $F_b(C_i)$ in order to fit experimental data more accurately, but using (3) does not change the model's qualitative behavior.

The cost for defense against predation in this system has been demonstrated to be a reduced ability to compete for scarce nutrients [24,29,47]. We model this by specifying a tradeoff curve

$$K_c(p) = K_c + \alpha_2(1 - p)^{\alpha_1}. \tag{4}$$

Here $K_c > 0$ is the minimum value of the half-saturation constant, $\alpha_1 > 0$ determines whether the tradeoff curve is concave up versus down, and $\alpha_2 > 0$ is the cost for becoming completely inedible ($p = 0$). The shape of the curve is unknown and thus is assumed here, but is unimportant for the purposes of this study. As discussed below, what matters for evolutionary and cryptic cycle properties is $K_c(0) - K_c(1)$, the relative half-saturation values of the two prey types.

3 Characteristics of the model under simulation

A system of more than 2 prey types invariably collapses to one or two types in the presence of a predator: either a single clone that outcompetes all others, or a pair of very different clones, one very well defended and the other highly competitive, that together drive all intermediate prey types to extinction [24,46]. Only the latter case is of final interest here, because with a single prey type there is no prey evolution. We thus consider a system of two extreme prey types in the presence of a predator.

Two system parameters can be experimentally varied: the dilution rate δ (fraction of the culture medium that is replaced daily) and the concentration of the limiting nutrient in the inflowing medium, N_I. Fussmann et al. [15] showed that δ is a bifurcation parameter: in both the real system and the model, the system goes to equilibrium at low dilution rates, limit cycles at intermediate dilution rates, and again to equilibrium at high dilution rates. Further increases in δ lead to extinction of the predator. Toth and Kot [43] proved that the same bifurcation sequence occurs in chemostat models with an age-structured consumer feeding on an abiotic resource (for our experimental system, the equivalent would be rotifers feeding on externally supplied algae that could not reproduce within the chemostat).

The prey vulnerability parameter p is also a bifurcation parameter. In the following discussion, we define *evolutionary cycles* as both prey types coexisting and exhibiting long-period cycles (period 20–40 days), with the predator and total prey abundance almost exactly out-of-phase with each other. *Cryptic cycles* are an extreme example of this dynamic which occurs if defense is both effective and very cheap [48].

Predator–prey cycles are shorter (6–12 days), display the classic quarter-period phase offset between predator and prey, and involve one prey type cycling with the predator. In addition, both prey may survive and coexist with the predator at an *evolutionary equilibrium*, or one prey type may be driven to extinction while the other goes to equilibrium with the predator.

Single prey model Figure 2a shows the dynamics of the single prey model as a function of prey palatability p and dilution rate δ. Parameters giving single-prey predator–prey cycles are indicated by open circles, and elsewhere the system goes to equilibrium. At low p values (up to 0.2–0.4, depending on the predator conversion efficiency χ_B) the system goes to equilibrium at all dilution rates. As p increases there is a bifurcation and short, low amplitude predator–prey cycles are observed, initially for the narrow range of dilution rates. When p is higher, oscillations grow in amplitude and increase very slightly in period, and cycling occurs over a larger range of dilution rates. The cycles always exhibit classic predator–prey phase relations.

Two prey models Figure 2b shows dynamics of the two prey model as a function of the dilution rate δ and the trait value p of the defended prey type (the model is scaled so that the undefended type has $p = 1$). Using the parameter values listed in Table 1, extended evolutionary cycles (closed circles) initially appear for all dilution rates ($0.2 \leq \delta \leq 1.3$) at p_1 very small ($p_1 \approx 0.01$). As p_1 increases, evolutionary cycling occurs for a diminishing range of dilution rates. By $p_1 \doteq 0.2$, cycling vanishes for all dilution rates, and instead the defended prey is in equilibrium (Fig. 2b, stipples) or the two prey types are in an evolutionary equilibrium with the predator (Fig. 2b, crosshatching). As p_1 increases further ($0.2 < p_1 < 1.0$, depending on dilution rate), there is another bifurcation and the system, comprised of the defended type and the predator, begins to exhibit predator–prey cycles (Fig. 2b, open circles). From this point on the system behaves as if it were dominated by the defended type (see above), until p_1 has increased to the point that the two prey types are almost identical. At that point there are predator–prey cycles with both prey types present (closed circles) but these appear to be very long transients rather than indefinite coexistence: one or the other prey type, depending on the dilution rate, is slowly driven to extinction by its competitor.

Effects of predator age structure. As the model fitted to our experimental data and used in prior studies includes age structure in the rotifer population, it is critical to the relevance of the present study that the reduced model (2) exhibits similar dynamics. In the full model, age structure is included by distinguishing between young, fecund rotifers and older, senescent rotifers. Fecund rotifers gradually senesce and cease reproductive activity at a rate $\lambda = 0.4$/day. Panels c and d in Fig. 2 shows model dynamics with age structure in the predator and all other parameters unchanged. As seen in Fig. 2c, the single prey model with age structure exhibits dynamics very similar to those in Fig. 2b, where age structure is not included. Predator age structure is generally stabilizing because senescent rotifers are a resource sink, eating prey without converting them to offspring. This effect is most pronounced at low values of δ because senescent rotifers then spend more time in the chemostat before getting

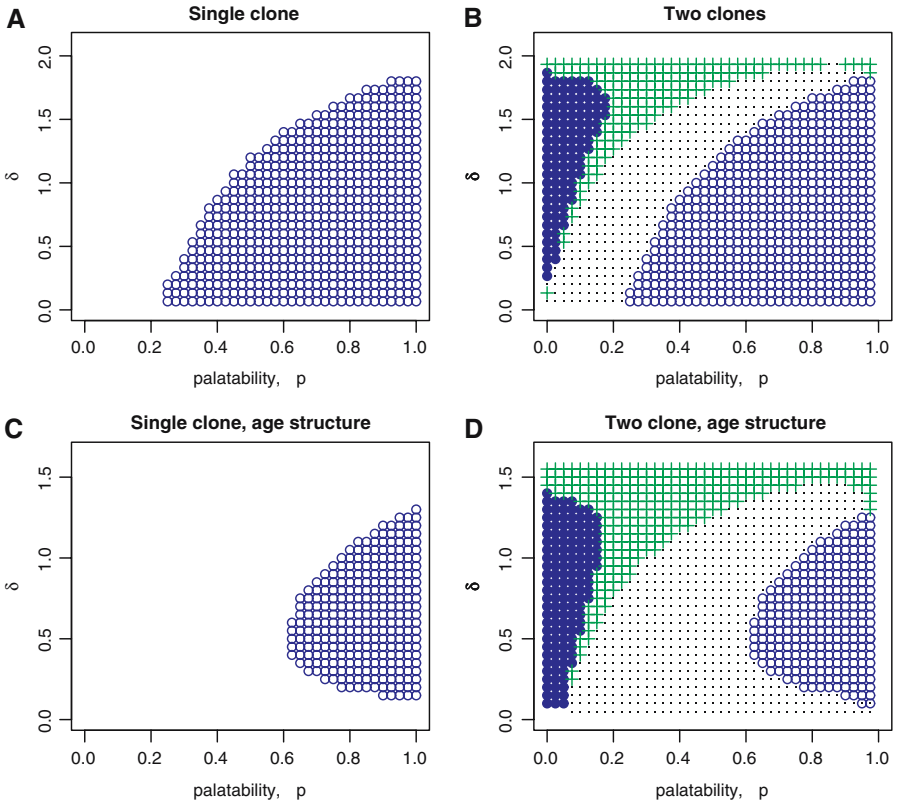

Fig. 2 Dynamics of one- and two-prey models as a function of the palatability p of the defended prey type and the dilution rate δ. **a** and **b** show results for the model without predator age structure (2). **c** and **d** show results for the full model including predator age structure (as in [24,46]). **a, c** Dynamics of a single prey system. *Open circles* show predator–prey cycles, and *white space* indicates equilibrium. **b, d** Dynamics of a two-prey system. The model is scaled so that the vulnerable prey type has $p = 1$. In the model with age structure (**d**), predator extinction occurs for $\delta > 1.5$. [Key: *filled circles* indicate that both types coexist and cycle together; *open circles* show short predator–prey cycles with only the defended type ($p < 1$). *cross-hatching* indicates the defended and vulnerable prey coexisting at a stable equilibrium; *stipples* indicate equilibrium between predator and defended prey, and *white space* indicates equilibrium between predator and vulnerable type.]

washed out. Omitting age structure is therefore destabilizing: it permits cycles with better defended prey (lower p) and eliminates entirely the stability at very low δ for nearly all p values. Similarly, simulations of the two-prey model show that eliminating predator age structure shifts the region of (p, δ) values giving evolutionary cycles to higher dilution rates, and eliminates the stabilization at very low δ, but otherwise the bifurcation diagram is unchanged.

4 Rescaling the model

We now simplify the model (1–3) by rescaling and further reducing its order. We order the prey types so that p_1 and p_2 correspond to the *defended* and *vulnerable* prey types,

respectively, $p_1 < p_2$. The cost for defense is reduced ability to compete for scarce nutrients, so $K_c(p_1) > K_c(p_2)$.

To rescale the model we make the following transformations:

$$S = \frac{N}{N_I}, \quad x_i = \frac{C_i}{\chi_c N_I}, \quad y = \frac{B}{\chi_c \chi_b N_I}, \quad g = \frac{\chi_b G}{\delta},$$
$$m = \frac{\chi_c \rho_c}{\delta}, \quad k_b = \frac{K_B}{\chi_c N_I}, \quad \tau = \delta t. \tag{5}$$

The half-saturation constants for each of the two prey types are transformed as follows,

$$k_1 = K_c(p_1)/N_I, \quad k_2 = K_c(p_2)/N_I. \tag{6}$$

Substituting these into equations (2) gives:

$$\begin{aligned} \dot{S} &= 1 - S - S \sum_{i=1}^{2} \frac{m x_i}{k_i + S} \\ \dot{x}_i &= x_i \left[\frac{mS}{k_i + S} - \frac{g p_i y}{k_b + Q} - 1 \right] \\ \dot{y} &= y \left[\frac{gQ}{k_b + Q} - 1 \right] \end{aligned} \tag{7}$$

where

$$Q = p_1 x_1 + p_2 x_2. \tag{8}$$

One more rescaling ($k_b \to k_b/p_2$, $p_1 \to p_1/p_2$) can also be done to set $p_2 = 1$ without loss of generality. Table 2 gives values of the rescaled model parameters corresponding to the parameter estimates in Table 1.

We can reduce the dimension of the system further by letting $\Sigma = S + x_1 + x_2 + y$. From (7) we have $\dot{\Sigma} = 1 - \Sigma$, so $\Sigma(t) \to 1$ quickly as $t \to \infty$. Thus, to study the long-term dynamics of (7), we may consider the dynamics on the invariant set $\Sigma \equiv 1$.

Table 2 Estimates of rescaled model parameters for the *Chlorella-Brachionus* microcosm system

Parameter	Description	Value
m	Algal maximum per-capita population growth rate	$3.3/\delta$
k_1, k_2	Algal half-saturation constants for nutrient uptake	0.054 (minimum)
g	Predator maximum grazing rate	$2.55/\delta$
k_b	Predator half-saturation constant for prey capture	0.21

Then $S(t) = 1 - x_1(t) - x_2(t) - y(t)$, and (7) reduces to

$$\begin{aligned} \dot{x}_i &= x_i \left[\frac{m(1-X-y)}{k_i + (1-X-y)} - \frac{g p_i y}{(k_b + Q)} - 1 \right], \quad i = 1, 2 \\ \dot{y} &= y \left[\frac{g Q}{k_b + Q} - 1 \right] \end{aligned} \tag{9}$$

where $X = x_1 + x_2$.

5 Analysis

Our goals in this section are to find the conditions under which two prey types can coexist, to determine when coexistence is steady-state versus oscillatory, and to characterize the period of cycles and the phase relations during oscillatory coexistence and during transients when one type is decreasing to extinction. Throughout this section we consider the reduced model (9). **Notation alert**: we use tildes (as in $\tilde{y}$) to indicate a three-way coexistence steady state (predator and both prey types), and overbars (as in $\bar{y}$) to indicate steady states with the predator and a single prey type. For local stability analysis it is useful to note that the model has the form

$$\dot{x}_i = x_i r_i(x_1, x_2, x_3), \quad i = 1, 2, 3 \tag{10}$$

with $x_3 = y$. It follows that at any equilibrium where the x_i are all positive (and hence the r_i are all 0) the Jacobian matrix J has entries

$$J(i, j) = \tilde{x}_i \frac{\partial \tilde{r}_i}{\partial x_j} \tag{11}$$

with the tilde indicating evaluation at the equilibrium with all x_i present. It is also useful for local stability analysis that the determinant of (11) is always negative unless $p_1 = p_2$ (Appendix D).

In this section we first briefly consider the dynamics of a system with one prey. We then use these results to analyze the dynamics of a system with two prey types, focusing on the conditions under which evolutionary cycles occur and the properties of those cycles. Because this section is necessarily technical and long, at the end (Sect. 5.4) we give a verbal summary of the results and their interpretation.

5.1 Dynamics of a one-prey system

We need first some properties of the one-prey model

$$\begin{aligned} \dot{x} &= x \left[\frac{m(1-x-y)}{k + (1-x-y)} - \frac{gpy}{(k_b + px)} - 1 \right] \\ \dot{y} &= y \left[\frac{gpx}{k_b + px} - 1 \right]. \end{aligned} \tag{12}$$

This is a standard predator–prey chemostat model and its behavior is well-known, so we summarize here only the results that we will need later; see e.g., [40] for derivations and details.

In the absence of predators, the steady state for this system is $E_0 = (1 - \Lambda, 0)$, where

$$\Lambda = \frac{k}{m-1}. \tag{13}$$

Λ is the scaled concentration of limiting nutrient at which prey growth balances washout rate, so that $\dot{x} = 0$. Similarly, steady state densities for each prey type in a predator-free two clone system are

$$E_i = (1 - \Lambda_i, 0) \quad \text{where} \quad \Lambda_i = \frac{k_i}{m-1}.$$

The steady state for the prey in the presence of the predator is

$$\bar{x}_c = \frac{k_b}{p(g-1)}; \tag{14}$$

$\bar{x}_c$ is the prey density at which the predator birth and death rates are equal. The model (12) has an interior equilibrium point $E_c = (\bar{x}_c, \bar{y}_c)$ representing predator–prey coexistence if

$$\Lambda + x_c < 1 \tag{15}$$

[40], and otherwise the predator cannot persist. The system then collapses to the prey by itself and converges to E_0. Condition (15) says that there is an interior equilibrium if the prey by themselves reach a steady state $(1 - \Lambda)$ that provides enough food so that the predator birth rate exceeds the predator death rate.

The expression for the steady state of the predator, y_c, is easily obtained from (12):

$$\bar{y}_c = \bar{\sigma} - \bar{x}_c, \quad \text{where} \quad \bar{\sigma} = (\bar{x}_c + \bar{y}_c) = \frac{1}{2}\left[\gamma - \sqrt{(\gamma^2 - 4m\bar{x}_c)}\right], \tag{16}$$

with $\gamma = k + 1 + m\bar{x}_c$. Similarly, the steady-state densities for the predator in a single-prey system with either prey type, $\bar{y}_i$, are found by substituting the steady state for the prey, $\bar{x}_i$, in place of $\bar{x}_c$ and the appropriate half-saturation k_i in place of k in (16).

We can use (15) to derive the condition for predator-prey coexistence in terms of the prey defense trait p and the dilution rate δ, recalling that Λ and x_c are both implicit functions of δ. Using (13) and (14) we obtain from (15)

$$\frac{k}{m(\delta) - 1} + \frac{k_b}{pg(\delta) - 1} < 1, \quad \text{or} \quad p > \frac{1}{1 - \Lambda}\left(\frac{k_b}{g(\delta) - 1}\right). \tag{17}$$

Note that the quantity within parenthesis above is the amount of substrate present in perfect food (undefended prey with $p = 1$). Solving (17) for δ in terms of p yields the boundary between predator extinction and stable coexistence in Figure 3. To the left of this line, the predator goes extinct and the equilibrium is E_0. As the left-hand side of the second expression in (17) is an increasing function of p, and the right-hand side is an increasing function of δ, the range of p values yielding coexistence narrows as δ increases (see Fig. 3).

As in the standard Rosenzweig–MacArthur predator–prey model, the stability condition has a graphical interpretation in terms of the nullclines. The prey nullcline is a parabola which peaks at

$$x^* = \frac{1}{m}\left[1 - k + \sqrt{\Lambda}(m-2)\right]. \tag{18}$$

The coexistence equilibrium is locally unstable if the peak of the prey nullcline is to the right of the predator nullcline (i.e., if $x^* > \bar{x}_c$). Note that a system with defended prey ($p < 1$) is always more stable than a system with fully vulnerable prey ($p = 1$) as reductions in p shift the predator nullcline to the right.

From (11) the Jacobian of (12) at E_c has the form

$$J_c = \begin{bmatrix} \bar{x}_c \frac{\partial \bar{r}_1}{\partial x} & - \\ + & 0 \end{bmatrix} \tag{19}$$

so E_c is locally stable if the trace $\mathbf{Tr}(J_c) = \bar{x}_c \frac{\partial \bar{r}_1}{\partial x}$ is negative. Cycles emerge through a Hopf bifurcation when the trace becomes positive. The condition $\mathbf{Tr}(J_c) \geq 0$ is equivalent to the following expression for model (12):

$$\frac{mk}{(k+1-\bar{x}_c-\bar{y}_c)^2} \geq \frac{gp^2\bar{y}_c}{(k_b+p\bar{x}_c)^2} \tag{20}$$

[40]. Cycles begin when the rates of change in prey substrate uptake (LHS) and in predator consumption (RHS) with respect to the amount of substrate present as prey (x) are exactly equal. Numerically solving (20) for δ in terms of p yields the boundary between stable coexistence and predator–prey cycles in Figure 3. It is known that these cycles are stable and unique near the Hopf bifurcation, and numerical evidence uniformly indicates that they are always unique and attract all interior initial conditions except E_c [40].

5.2 Stability and dynamics of a two-prey system

System (9) has two prey types ordered so that $0 < p_1 < p_2 = 1$. We refer to prey 1 as the *defended* type and prey 2 as the *vulnerable* type. The cost for defense comes in the form of reduced growth rate, $1/k_1 \leq 1/k_2$.

Following Abrams [2], we begin by finding the conditions for existence of an equilibrium $(\tilde{x}_1, \tilde{x}_2, \tilde{y})$ at which all three population densities are positive; we refer to this

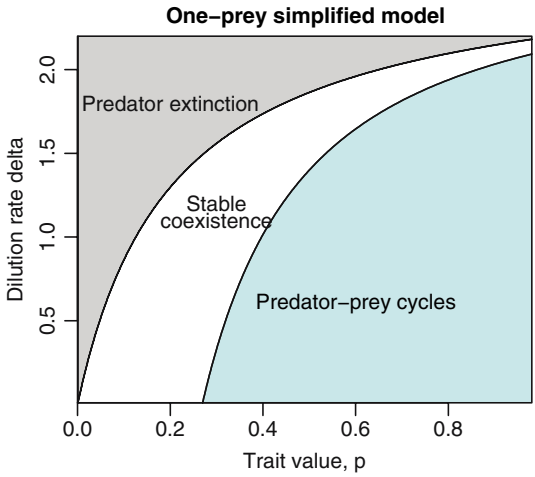

Fig. 3 Bifurcation diagram for the rescaled, reduced clonal model with one prey type

as a *coexistence equilibrium*. Setting (9) to zero and solving gives expressions for $\tilde{X}$, $\tilde{Q}$ and $\tilde{y}$ in terms of model parameters (see Appendix C; as above $Q = p_1x_1 + p_2x_2$ is the total prey quality, and $X = x_1 + x_2$ is the total prey density). The prey steady states $\tilde{x}_1, \tilde{x}_2$ are then

$$\begin{bmatrix} \tilde{x}_1 \\ \tilde{x}_2 \end{bmatrix} = \frac{1}{p_2 - p_1} \begin{bmatrix} p_2\tilde{X} - \tilde{Q} \\ \tilde{Q} - p_1\tilde{X} \end{bmatrix}. \tag{21}$$

where

$$\tilde{Q} = \frac{k_b}{g - 1}. \tag{22}$$

A coexistence equilibrium thus exists provided $\tilde{X} > 0$ and $p_1\tilde{X} < \tilde{Q} < p_2\tilde{X}$, or

$$p_1 < \frac{\tilde{Q}}{\tilde{X}} < p_2. \tag{23}$$

Beyond the above, system (9) does not yield tidy analytical solutions for the steady states at coexistence. To study how parameter variation affects coexistence, we start by graphically mapping the region where a coexistence equilibrium exists as a function of the defended clone's parameters, p_1 and k_1 (Fig. 4), without regard to whether or not the equilibrium is locally stable. The coexistence region also varies with δ, but selecting several δ values of interest gives a general sense of how the coexistence region varies as a function of dilution rate.

The lower boundary of the coexistence region occurs when the cost of defense is so high that the equilibrium density of the defended prey x_1 drops to zero while x_2 and y remain positive. Recalling the general form (10), the lower boundary is thus defined

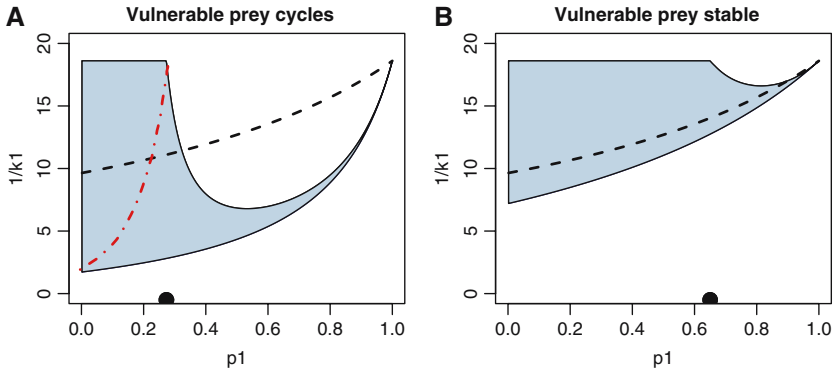

Fig. 4 Prey coexistence equilibria. The shaded regions indicate parameters $(p_1, 1/k_1)$ for prey type 1 giving a coexistence equilibrium (stable or unstable) with the vulnerable prey type $p_2 = 1$. At $\delta = 1.5$ **a** Prey type 2 cycles, and at $\delta = 2.0$. **b** Prey type 2 is stable. A solid point on the p_1 axis marks $p_1 = p^*$ in each panel. The *dashed lines* show a representative tradeoff curve (4), assuming roughly 50% reduction in growth rate as the cost of being 100% defended. Here $k_c = 0.054$, $\alpha_1 = 1.0$, and $\alpha_2 = 0.05$. In **a** the *dash-dotted line* delimits where the defended type can invade the limit cycle of the predator and vulnerable prey type. For k_1 sufficiently small (i.e., above the line) the defended prey type can invade the limit cycle, below the line it cannot invade

by the conditions

$$r_1(0, x_2, y) = r_2(0, x_2, y) = r_3(0, x_2, y) = 0 \quad \text{with } x_2 > 0, y > 0.$$

The conditions on r_2 and r_3 are satisfied by the steady state $E_2 = (0, \bar{x}_2, \bar{y}_2)$ for a one-prey system with only the vulnerable prey. The lower boundary of the coexistence region is then defined by the condition $r_1(0, \bar{x}_2, \bar{y}_2) = 0$, which can be written as

$$\frac{1}{k_1} = \frac{1}{1 - \bar{x}_2 - \bar{y}_2} \left[\frac{\bar{y}_2 p_1 + \bar{x}_2}{\bar{x}_2(m-1) - \bar{y}_2 p_1} \right]. \tag{24}$$

The upper boundary of the coexistence region occurs when the cost of defense is so low that the defended prey (at the equilibrium density) drives one of the other populations to extinction. In Sect. 6 we show that for $p_1 < p^* = \tilde{Q}/\bar{x}_2$, the predator goes extinct first ($\tilde{y} \to 0$) as k_1 decreases, because the defended prey (at steady state) drives the vulnerable prey to low abundance and the defended prey is very poor food. This occurs at $k_1 = k_2$ (zero cost of defense). For $p_1 > p^*$, the vulnerable prey type is outcompeted by the defended type before k_1 has reached k_2. This boundary is therefore defined by the conditions

$$r_1(x_1, 0, y) = r_2(x_1, 0, y) = r_3(x_1, 0, y) = 0 \quad \text{with } x_1 > 0, y > 0.$$

The conditions on r_1 and r_3 are solved by the one-prey steady state $E_1 = (\bar{x}_1, 0, \bar{y}_1)$, so the condition $r_2(\bar{x}_1, 0, \bar{y}_1) = 0$ defines the upper boundary of the coexistence region

for $p > p^*$. The upper boundary of the coexistence region is thus the curve

$$\frac{1}{k_1} = \min\left[\frac{1}{k_2}, \frac{1}{\varphi(\bar{x}_1, \bar{y}_1)}\right] \tag{25}$$

where φ is value of k_1 that solves

$$\frac{m(1-\bar{x}_1-\bar{y}_1)}{k_2+(1-\bar{x}_1-\bar{y}_1)} - \frac{\bar{y}_1 + p_1\bar{x}_1}{(p_1\bar{x}_1)} = 0, \tag{26}$$

noting that $\bar{x}_1$ and $\bar{y}_1$ are functions of k_1 and p_1. The two segments of the upper boundary defined by (25) meet at the point

$$p_1 = p^* = \frac{\bar{Q}}{\bar{x}_2} = \frac{\bar{Q}}{1-\Lambda_2}, \quad k_1 = k_2.$$

As $\delta \to 0$ (with the parameter scalings in Table 2), $\bar{Q} \to 0$ and $\Lambda_2 \to 0$, thus $p^* \to 0$. So as $\delta \to 0$ there typically an increasingly narrow band of p_1 values for which a $p_1 - k_1$ tradeoff curve lies in the coexistence equilibrium region, unless by chance the tradeoff curve lies exactly inside the cusp of the coexistence equilibrium region.

As $p_1 \to 1$, the upper and lower boundaries of the coexistence region meet at $p_1 = p_2 = 1, k_1 = k_2$ (Fig. 4). That is, if the two prey are almost equally vulnerable to predation, they can only coexist at equilibrium if a tiny bit of defense has a tiny cost. To prove that this occurs, we show that the point $p_1 = 1, k_1 = k_2$ lies on both boundaries. At this point the two prey are identical so $\bar{x}_1 = \bar{x_2}$ and $\bar{y}_1 = \bar{y}_2$.

The upper boundary is defined by $r_2(\bar{x}_1, 0, \bar{y}_1) = 0$. At $p_1 = 1$ and $k_1 = k_2$, $r_2(\bar{x}_1, 0, \bar{y}_1) = r_2(\bar{x}_2, 0, \bar{y}_2) = r_2(0, \bar{x}_2, \bar{y}_2) = 0$, thus $p_1 = 1, k_1 = k_2$ lies on the upper boundary.

The lower boundary is defined by $r_1(0, \bar{x}_2, \bar{y}_2) = 0$. At $p_1 = 1$ and $k_1 = k_2$, $r_1(0, \bar{x}_2, \bar{y}_2) = r_1(0, \bar{x}_1, \bar{y}_1) = r_2(\bar{x}_1, 0, \bar{y}_1) = 0$, which shows that $p_1 = 1, k_1 = k_2$ also lies on the lower boundary. Thus both boundaries converge to $k_1 = k_2$ as $p_1 \to 1$.

5.3 Local stability analysis

To characterize two-prey evolutionary cycles we need to find the bifurcation curves in parameter space where these cycles arise. The "empirical facts" are summarized in Fig. 5, based on numerical evaluations of the Jacobian and its eigenvalues within the coexistence equilibrium region. In Fig. 5 we change the stability of the (predator + vulnerable prey) system by varying the value of δ, but the results are qualitatively the same if other parameters are varied instead (e.g., varying the prey maximum growth rates).

The stability properties in Fig. 5 explain the major qualitative features of the two-prey model's bifurcation diagram (Fig. 2d). To see the connection, recall that a horizontal (constant δ) slice through Fig. 2d corresponds to a tradeoff curve between

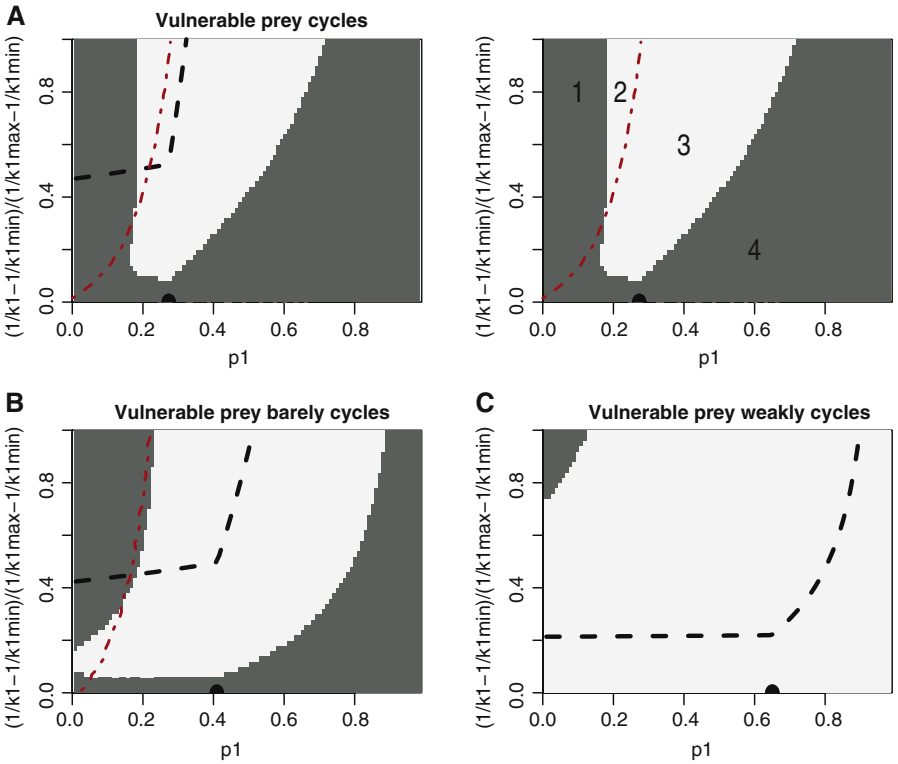

Fig. 5 Stability of coexistence equilibria for the reduced two-prey model. In each panel, the *horizontal axis* is the palatability p_1 of the defended prey with the model scaled so that $p_2 = 1$. To remain consistent with Abrams (cf. [2], Figs. 1–3) the vertical axis is $1/k_1$, scaled so that 0 and 1 correspond to the lower and upper limits of the coexistence equilibrium region (Fig. 4). The Jacobian matrix and its eigenvalues were evaluated at an even 50×100 grid of values. *Lighter gray* indicates that the equilibrium is stable, *darker gray* that it is unstable; in all cases the computed eigenvalues with largest real part are a complex conjugate pair. A *solid semicircle* on the p_1 axis marks $p_1 = p^*$, the value where the straight and curved segments of the upper limit of the coexistence equilibrium region meet. The *dashed curve* in panels a and b is the tradeoff curve $k_1 = k_c + \alpha_2(1 - p_1)^{\alpha_1}$, with $k_c = k_2 = 0.054, \alpha_1 = 1; \alpha_2 = 0.05$ at p_1 values lying within the coexistence equilibrium region. The *dash-dotted line* represents the minimum $1/k_1$ values at which the defended prey can invade the (predator + vulnerable prey) limit cycle (see Appendix E). Parameter values for these plots are as follows: **a** $\delta = 1.5$; **b** $\delta = 1.75$; **c** $\delta = 2.0$. All other parameters are unchanged and are as shown in Table 2. To the right of **a** is a key to the dynamics shown in this figure: *1* predator + vulnerable prey cycle, and their limit cycle is invasible $\Rightarrow$ evolutionary cycling; *2* stable coexistence equilibrium; predator + vulnerable prey limit cycle is invasible $\Rightarrow$ steady state coexistence of three types; *3* stable coexistence equilibrium; predator + vulnerable prey limit cycle is *not* invasible $\Rightarrow$ multiple attractors (coexistence steady state, classic predator–prey cycles); and *4* predator + vulnerable prey cycle, and their limit cycle is *not* invasible $\Rightarrow$ classic predator–prey cycles

p_1 and k_1 in the panel of Fig. 5 with the same value of δ. Panel a of Fig. 5 has $\delta = 1.5$. When p_1 is near 1, the tradeoff curve lies above the coexistence equilibrium region, and the defended prey type eventually outcompetes the vulnerable type. For p_1 very close to 1 the prey types are very similar, and the vulnerable type persists for a long time. The system exhibits "classical" predator–prey cycles as if a single prey-type were present, even though two types are transiently coexisting. For p_1 somewhat smaller,

the vulnerable type is quickly eliminated and there are either classical cycles with only the defended type (open circles in Fig. 2d), or (for lower values of p_1) the defended prey type goes to a stable equilibrium with the predator (open triangles in Fig. 2d). As p_1 decreases further, Fig. 5a shows that the tradeoff curve enters the coexistence region in the area where the coexistence equilibrium is stable, so the system then exhibits stable coexistence (cross-hatching in Fig. 2d). Finally, as p_1 decreases towards 0, the tradeoff curve enters the area where the coexistence equilibrium is unstable, and it lies above the dash-dot curve marking the k_1 value required for the defended prey type to invade the vulnerable prey's limit cycle with the predator. The system exhibits evolutionary cycles with both prey types persisting (filled circles at $p \approx 0$ in Fig. 2d).

Figure 5a also shows that there is a region of parameters (below the dash-dot curve) where the coexistence equilibrium is stable and the system therefore has coexisting attractors: a locally stable coexistence equilibrium, and a locally stable limit cycle with the predator and the vulnerable prey.

Figure 5b, which has $\delta = 1.75$, shows the same sequence of transitions as Fig. 5a, but each occurs at higher values of p_1, reflecting the stabilizing effect of increased washout. This is reflected in Fig. 2d: increasing δ above 1.0 shifts all the bifurcation boundaries to higher p values, but the sequence of bifurcations as p decreases is unchanged. However for δ sufficiently high (panels c and d in Fig. 5), the tradeoff curve lies either below the coexistence equilibrium region or within the region where the coexistence equilibrium is stable, so evolutionary cycles never occur. Instead, there is either stable coexistence of the two prey with the predator, or classical predator–prey cycles with only the vulnerable prey type.

Evolutionary cycles are also eliminated—but for a different reason—as $\delta \downarrow 0$ in Fig. 2d. As noted above, as $\delta \downarrow 0$ we also have $p^* \downarrow 0$, so unless $p_1 \approx 0$ the tradeoff curve lies above the coexistence equilibrium region and only the defended prey persists with the predator, cycling at higher p_1 and stable at lower p_1. Only very near $p_1 = 0$, a region tiny enough to be missed by our simulation grid in Fig. 2, can there be coexistence of both prey with the predator.

Stability on the edges. We can gain some understanding of the patterns in Fig. 5, and see that they are not specific to the parameter values used to draw the figure, by examining the limiting cases that occur along the edges of the coexistence equilibrium region. One general conclusion (explained below) is that the bottom and right edges, and the right-hand portion of the top edge, all must have the same stability as the reduced system with the predator and only the vulnerable prey (prey type 2). However even if this system is unstable, there must be a region along the top edge where the coexistence equilibrium is stable.

The Jacobian matrix that determines equilibrium stability is derived in Appendix D. We also show there that the determinant of this Jacobian is always negative at a coexistence equilibrium unless $p_1 = p_2$, so the coefficient $c_0 = -\det(J)$ in the Routh–Hurwitz stability criterion for 3-dimensional systems is always positive.

Bottom and right edges Near the bottom and right edges, the coexistence equilibrium has the same local stability as the (predator + vulnerable prey) subsystem (panels a and b versus c and d in Fig. 5). The bottom edge is the lower limit of the coexistence

equilibrium region, where $\tilde{x}_1 \to 0$. The coefficients for the Routh–Hurwitz stability criterion (see Appendix B) are then

$$c_0 = -\det(J) > 0, \quad c_1 = T_2(J) \to \delta_2, \quad c_2 = -T(J) \to -\tau_2 \tag{27}$$

where δ_2 and τ_2 are the determinant and trace, respectively, of the 2×2 Jacobian for the (predator + vulnerable prey) system, and T_2 is the sum of all order-2 principal minors (Appendix B). If this one-prey system is stable then $\delta_2 > 0$, $\tau_2 < 0$ so c_0, c_1 and c_2 are all positive. Moreover $c_0 = O(\tilde{x}_1)$ (see Appendix D), so when $\tilde{x}_1$ is small we have $c_1 c_2 > c_0$ and the equilibrium is stable. Conversely if the steady state for the (predator + vulnerable prey) system is unstable, c_2 is negative so the full system is also unstable.

The right edge corresponds to the cusp in the coexistence region as $p_1 \to 1$. Near the cusp the two prey become increasingly similar ($p_1 \approx p_2 = 1, k_1 \approx k_2$). Using (11), the functional forms of the r_i (10) and the fact that $p_1 \approx p_2$ imply that the form of J is approximately

$$J_0 = \begin{bmatrix} aq & aq & -qb \\ a(1-q) & a(1-q) & -(1-q)b \\ c & c & 0 \end{bmatrix} \tag{28}$$

where $q = \tilde{x}_1/(\tilde{x}_1 + \tilde{x}_2)$; even if p_1 is near p_2, it is not necessarily the case that $\tilde{x}_1$ is close to $\tilde{x}_2$. In (28) b and c are positive while a has the sign of $\partial r_1/\partial x_1$ which may be positive or negative. One eigenvalue of J_0 is 0, corresponding to the dynamics of $x_1 - x_2$. The others are $\frac{1}{2}(a \pm \sqrt{a^2 - 4bc})$, which are also the eigenvalues of a single-prey system at the coexistence steady state. Thus, the two-prey system with $p_1 \approx p_2 = 1$ "inherits" two eigenvalues from the one-prey system with $p = 1$.

When the one-prey system with $p = 1$ is cyclic, the inherited eigenvalues are a complex conjugate pair. In the corresponding eigenvectors, the components for the two clones are identical when $p_1 = p_2$. This implies that when $p_1 \approx p_2$ the eigenvector components will be similar, so the two prey types cycle almost exactly in phase. The period of these oscillations is determined by the inherited eigenvalues, so it is close to the period of the corresponding one-prey system.

When the one-prey system is stable, the Routh–Hurwitz criterion (Appendix B), using J_0 to approximate trace(J) and $T_2(J)$ and the fact that $\det(J) < 0$ for $p_1 \neq p_2$, implies that the full system will also be stable. Therefore, a coexistence equilibrium with two nearly identical prey has the same stability as the equilibrium for the corresponding one-prey systems. During damped oscillations onto a stable coexistence equilibrium, or diverging oscillations away from an unstable one, the clones will oscillate nearly in phase with each other and inherit the cycle period of the one-prey system.

Top edge The rightmost portion of the top edge also corresponds to the cusp in the coexistence equilibrium region, so the stability here is also the same as that of the (predator + vulnerable prey) system. In general, as $1/k_1$ approaches the upper limit of the coexistence equilibrium region when $p_1 > p^*$ (the curved portion), the stability

of the two-prey system approaches that of the (predator + defended prey) system with $1/k_1$ approaching $1/k_2$. This must be stable if the (predator + vulnerable prey) system is stable, because the defended prey is always more stable, as noted above. If the (predator + vulnerable prey) system cycles, then there will be instability as $p_1 \to 1$ along the top edge.

However, there is always stability near the top edge for $p_1 \to p^*$, as follows. Along the straight portion of the top edge ($p_1 < p^*$), as $1/k_1$ approaches the edge, the coexistence equilibrium converges to a limit with $\tilde{y} = 0$, while along the curved portion the limiting coexistence equilibrium has $\tilde{x}_2 = 0$. So near their intersection at $p_1 = p^*$, both $\tilde{x}_2$ and $\tilde{y}$ approach 0. Condition (20) then implies that the (predator + defended prey) system is stable, so the coexistence equilibrium is stable near the top edge for p_1 just above p^*. By continuity, there is an open region of (p_1, k_1) values near $p_1 = p^*, k_1 = k_2$ where the coexistence equilibrium is locally stable. If the (predator + vulnerable prey) system is only weakly unstable then this stability region may be quite large (Fig. 5b), but it cannot reach either the bottom or right edges.

Left edge Finally, consider the left edge at $p_1 = 0$. The steady states simplify to

$$\tilde{x}_1 = 1 - \tilde{Z} - \tilde{x}_2 - \tilde{y}, \quad \tilde{x}_2 = \tilde{Q} = \frac{k_b}{g-1}, \quad \tilde{y} = \tilde{Q}(m-1)\frac{(k_1 - k_2)}{k_1 + k_2(m-1)} \tag{29}$$

where $\tilde{Z} = \frac{k_1}{m-1}$. The coexistence equilibrium exists for $\vartheta < \frac{1}{k_1} < \frac{1}{k_2}$ where ϑ is the value of $1/k_1$ that solves $\tilde{x}_2 + \tilde{y} + \tilde{Z} = 1$, noting that $\tilde{y}$ depends on k_1. The Jacobian matrix at (29) is

$$J = \begin{bmatrix} -a_1\tilde{x}_1 & -a_1\tilde{x}_1 & -a_1\tilde{x}_1 \\ -a_2\tilde{x}_2 & (-a_2 + g\tilde{y}F^2)\tilde{x}_2 & -(a_2 + gF)\tilde{x}_2 \\ 0 & gk_b\tilde{y}F^2 & 0 \end{bmatrix} \tag{30}$$

where setting $p_1 = 0$ and $p_2 = 1$ gives $F = \frac{1}{k_b + \tilde{x}_2}$ and

$$a_i = \frac{mk_i}{(k_i + \tilde{Z})^2}. \tag{31}$$

Near the lower limit of the left edge, we know that the system inherits the stability of the (predator + vulnerable prey) system. Above the lower limit we can use the Routh–Hurwitz criterion (Appendix B) to determine stability. The coefficients c_0 and c_1 have common factor $\tilde{x}_2 g F^2 > 0$. Dividing this out gives modified coefficients

$$\tilde{c}_0 = a_1\tilde{x}_1 g k_b F > 0, \quad \tilde{c}_1 = k_b(a_2 + gF) - a_1\tilde{x}_1, \quad \tilde{c}_2 = a_1\tilde{x}_1 + \tilde{x}_2(a_2 - g\tilde{y}F^2) \tag{32}$$

and the stability conditions remain the same: $\tilde{c}_0,\ \tilde{c}_1,\ \tilde{c}_2 > 0,\ \tilde{c}_1\tilde{c}_2 > \tilde{c}_0$. Extensive numerical evaluations of the coefficients as δ is varied indicate that loss of stability occurs when the condition $\tilde{c}_1\tilde{c}_2 - \tilde{c}_0 > 0$ is violated—the equilibrium is stable if this

condition holds and unstable if it fails. Assuming this is true, loss of stability along the left edge occurs via a Hopf bifurcation (Appendix B). Global persistence results for the model with $p_1 = 0$ were obtained by Butler and Wolkowicz [12].

5.4 The structure of evolutionary cycles

The stability analysis above delimits the situations in which evolutionary cycles occur. As illustrated in Fig. 5a, they arise when the p_1 versus k_1 tradeoff curve passes (with decreasing p_1) from the region of stable coexistence equilibria near $p_1 = p^*, k_1 = k_2$ to the region of unstable coexistence equilibria with $p_1 \approx 0$. For $1/k_1$ below the dash-dot curve in Fig. 5a, the defended prey cannot invade the vulnerable prey–predator limit cycle (see Fig. 6). As $1/k_1$ increases, the defended prey becomes persistent and then increases in average abundance. As $1/k_1 \to 1/k_2$ the characteristic features of evolutionary cycles emerge: longer cycle period and out-of-phase oscillations in predator and total prey abundance.

To understand the phase relations on evolutionary cycles, we need to examine the dominant eigenvector of the Jacobian matrix for the unstable fixed point (Fig. 7). There

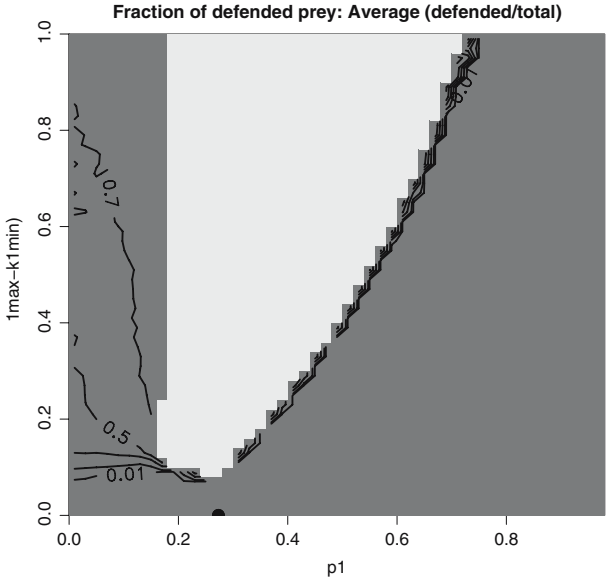

Fig. 6 Contour plot of the long-term average fraction of defended prey. The *horizontal axis* is the palatability p_1 of the defended prey, with the model scaled so that $p_2 = 1$. The vertical axis represents $1/k_1$, with 0 and 1 corresponding to the lower and upper limits of the coexistence equilibrium region (Fig. 4). Numerical solutions of the model were used to compute the long-term average value of $x_1/(x_1 + x_2)$ for parameter values such that the (predator + vulnerable prey) system (same parameter values as panel a of Fig. 5). In the *lighter-gray region* the coexistence equilibrium is stable. In the *darker-gray region* the equilibrium is unstable. The *vertical black line* is at $p_1 = p^*$, the value where the straight and curved segments of the upper limit of the coexistence equilibrium region meet. The *dash-dot line* is the minimum $1/k_1$ value at which the defended prey can invade the (predator + vulnerable prey) limit cycle. Parameter values are as in Table 2 with $\delta = 1.0$

is a codominant pair of complex conjugate eigenvalues, and (because $\det(J) < 0$) the third eigenvalue is real and negative. When the defended prey has very low palatability, the predator and the vulnerable prey have the classical quarter-period phase lag. Here the phase angle is 90°; because eigenvectors are only defined up to arbitrary scalar multiples, including arbitrary rotations in the complex plane from multiplication by $e^{i\theta}$, only the relative phases of eigenvector components are meaningful. As $1/k_1$ increases, the eigenvector components for the two prey types become out of phase with each other ($\approx 180°$ phase angle, right column of Fig. 7). As a result, the predator and total prey densities are out of phase with each other.

In the next section we show that these phase relations become exact as the limit $1/k_1 \to 1/k_2$ is approached, for a general version of the model which does not specify the functional forms of the predator and prey functional responses.

The four "right angle" phase relations that arise as the cost of defense becomes vanishingly small explain the most obvious qualitative feature of evolutionary cycles. Specifically, it implies that predator and prey densities are exactly out of phase, in a way that cannot occur in a standard predator–prey model without prey evolution because it would violate existence and uniqueness of solutions. In the next section, we show mathematically that these phase relations become exact as the cost of defense drops to zero, for a general version of the model in which we do not specify the functional forms of the predator and prey functional responses. Analysis of the general model also provides explanations for the long period of evolutionary cycles, and for the emergence of "cryptic cycles" (as in Fig. 1b) when the cost of defense is low. The transition from evolutionary to cryptic cycles is gradual, with cycle period lengthening and variability in total prey decreasing as the cost of defense decreases. The next section is the most technical in the paper, and it can be skipped on first reading. The main conclusion is as summarized above: the important features of evolutionary cycles are a consequence of the biologically realistic (but rarely made) assumption that effective defense can be cheap.

6 Evolutionary cycles in a general two-prey model

In this section we analyze the limiting properties of evolutionary cycles, for $p_1 \ll 1$ and low cost to defense, without specifying the functional forms of the prey and predator functional responses. We consider a two-prey, one-predator model that (after rescaling) can be written in the form

$$\begin{aligned} \dot{x}_i &= x_i \left(f(X, y, \theta_i) - p_i y g(Q) \right), \quad i = 1, 2 \\ \dot{y} &= y \left(Q g(Q) - d \right) \end{aligned} \tag{33}$$

where $X = x_1 + x_2$ is the total density of prey and $Q = p_1 x_1 + p_2 x_2$ is the total prey quality as perceived by the predator. The key assumption in (33) is total niche overlap in the prey types (e.g., because they are two clones within a single species), which is reflected in f being a function of X. To model the trophic relations, f is assumed to be strictly decreasing in X and nonincreasing in y, and $h(Q) = Qg(Q)$ is strictly increasing in Q. Specific examples of the general model (33) include the two-prey,

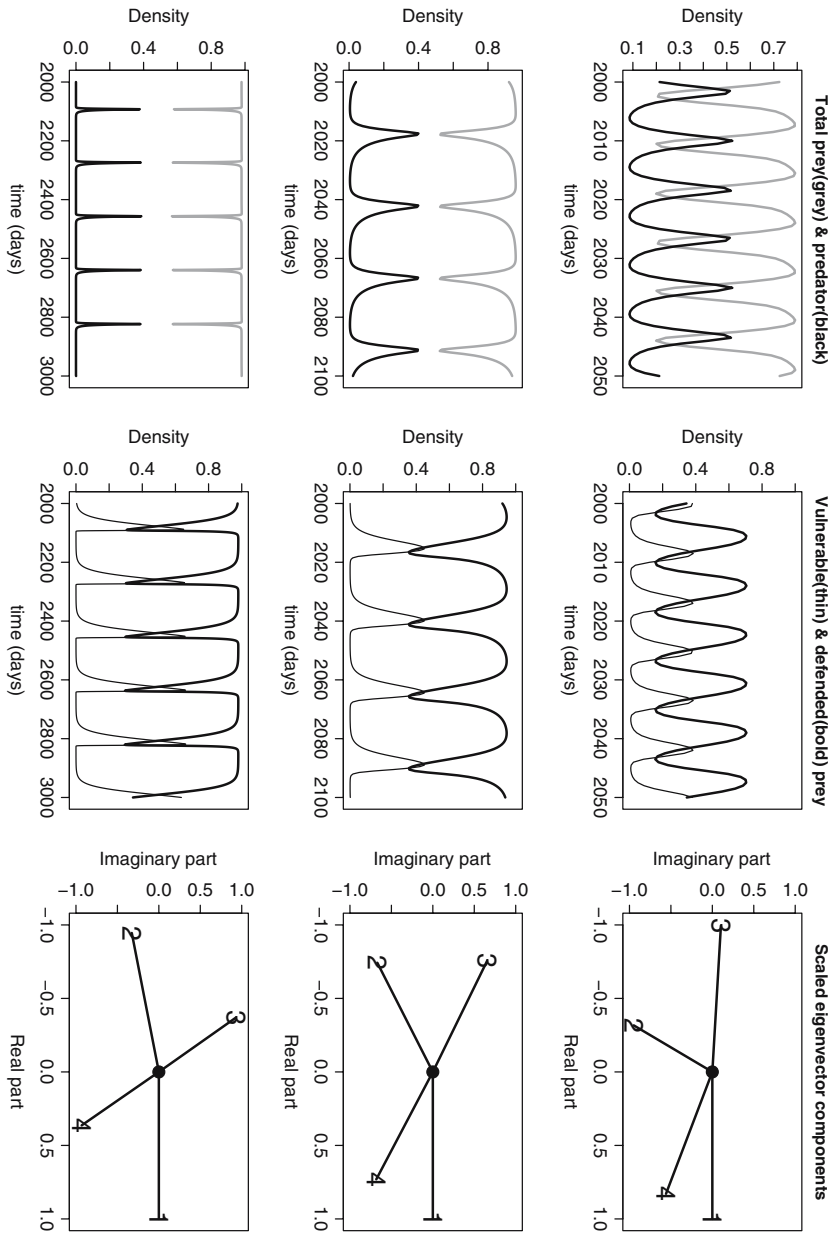

Fig. 7 Coexistence of edible and defended prey on a limit cycle. Parameter values for all plots were $\delta = 0.9, m = 3.3/\delta, g = 2.3/\delta, k_2 = 0.05, k_b = 0.2, p_2 = 1, p_1 = 0.08$. Values of k_1 were 0.4 (*top row*), 0.1 (*center row*) and 0.055 (*bottom row*). In each row the *leftmost panel* shows the dynamics of total prey and predator densities, the *center panel* shows the dynamics of the two prey types, and the rightmost panel shows the phases of the Jacobian dominant eigenvector components: *1* defended prey, *2* edible prey, *3* predator, *4* total prey

one-predator chemostat model analyzed in the previous section of this paper, and the Abrams–Matsuda model [1], which is a two-prey version of the classic Rosenzweig–MacArthur model with Lotka–Volterra competition between the prey.

In (33), let θ be some parameter affecting the ability of the prey to compete for nutrients. We assume that f is increasing in θ. Then to simplify notation and without loss of generality we take θ to be the steady-state density for a single prey type in the absence of predators, i.e.,

$$f(\theta, 0, \theta) = 0. \tag{34}$$

As usual we take $p_1 < p_2 = 1$. We therefore assume that $\theta_1 < \theta_2$ because of the tradeoff between defense and competitive ability.

In the chemostat model, the situation giving rise to evolutionary cycles is when $\theta_1 \uparrow \theta_2$ with $p_1 \ll 1$. Evolutionary cycles are generated by the following two properties:

1. There is a positive coexistence equilibrium with $\tilde{x}_1, \tilde{x}_2$ converging to positive limits while $\tilde{y} \to 0$ as $\theta_1 \uparrow \theta_2$;
2. The coexistence equilibrium is a spiral for $\theta_1 \approx \theta_2$.

In Appendix F we show that these properties of the chemostat model also hold in the general model (33) for p_1 sufficiently small and θ_1 sufficiently near θ_2. Evolutionary cycles then occur whenever the coexistence equilibrium is unstable. Evolutionary cycles are thus a general property of (33) rather than a special property of the chemostat model.

To determine the limiting phase relations as $\theta_1 \uparrow \theta_2$, we need to find the eigenvector corresponding to the dominant eigenvalue with positive imaginary part. The relative phase angles of this eigenvector's components (in the complex plane) correspond to the phase lags between the corresponding state variables in solutions to the linearized system near the steady state (see Appendix A). The Jacobian for (33) in the limit $\theta_1 \uparrow \theta_2$ is

$$J_0 = \begin{bmatrix} \tilde{x}_1 \tilde{f}_X & \tilde{x}_1 \tilde{f}_X & \tilde{x}_1 f_y - p_1 \tilde{x}_1 \tilde{g} \\ \tilde{x}_2 \tilde{f}_X & \tilde{x}_2 \tilde{f}_X & \tilde{x}_2 f_y - \tilde{x}_2 \tilde{g} \\ 0 & 0 & 0 \end{bmatrix}. \tag{35}$$

The characteristic polynomial of (35) factors to show that the eigenvalues of (35) are $f_X(\tilde{x}_1 + \tilde{x}_2) < 0$ and 0 as a repeated root. The eigenvector for the negative eigenvalue is $(\tilde{x}_1, \tilde{x}_2, 0)$, and for 0 there is the unique eigenvector $(1, -1, 0)$. The zero eigenvalue therefore has algebraic multiplicity 2 and geometric multiplicity 1.

To determine the limiting phase relations in evolutionary cycles consider a small perturbation off the limit of the defended prey parameters, $\theta_1 = \theta_2 - \epsilon$. For ϵ small, we show in Appendix F that the double-zero eigenvalue is perturbed to a complex conjugate pair of eigenvalues. To study cycles we assume that the eigenvalues have positive real part. That is, near the double-zero root the (scaled) characteristic polynomial is perturbed to leading order from $p(z) = z^2$ to $p(z) = (z - \epsilon a)^2 + \epsilon b^2$ for some $b > 0$. The perturbed eigenvalues therefore have $O(\epsilon)$ real part and imaginary parts $\pm\sqrt{\epsilon} bi$ to leading order (here $i = \sqrt{-1}$).

We need to determine the corresponding perturbed eigenvectors. Let $\mathbf{w_0}$ denote the unperturbed eigenvector $(1, -1, 0)$, and let $\mathbf{w_0} + \mathbf{w_e}$ be a perturbed eigenvector corresponding to the complex eigenvalue with positive imaginary part, scaled so that its first component is 1. The first component of $\mathbf{w_e}$ is therefore 0. The perturbed Jacobian is $J_0 + \epsilon J_1$ for some matrix J_1. Then

$$(J_0 + \epsilon J_1)(\mathbf{w_0} + \mathbf{w_e}) = \sqrt{\epsilon} bi(\mathbf{w_0} + \mathbf{w_e}) + O(\epsilon). \tag{36}$$

Using $J_0\mathbf{w_0} = 0$ and keeping only leading-order terms, gives

$$J_0\mathbf{w_e} = \sqrt{\epsilon} bi\mathbf{w_0}. \tag{37}$$

Let $\mathbf{w_e} = (0, w_2, w_3)$; then writing out (37) in full, w_2 and w_3 satisfy

$$\begin{bmatrix} \tilde{x}_1 f_X & \tilde{x}_1 f_y - p_1 \tilde{x}_1 \tilde{g} \\ \tilde{x}_2 f_X & \tilde{x}_2 f_y - \tilde{x}_2 \tilde{g} \end{bmatrix} \begin{bmatrix} w_2 \\ w_3 \end{bmatrix} = \sqrt{\epsilon} bi \begin{bmatrix} 1 \\ -1 \end{bmatrix}. \tag{38}$$

w_2 and w_3 must be purely imaginary, because the unique solution to the real part of (38) is $(0, 0)$. Writing $w_j = (\sqrt{\epsilon} bi) z_j$ and solving for the z's, we find that $z_2 < 0$ and $z_3 > 0$; specifically

$$\begin{bmatrix} z_2 \\ z_3 \end{bmatrix} \propto \begin{bmatrix} (\tilde{x}_1 + \tilde{x}_2) f_y - (p_1 \tilde{x}_1 + \tilde{x}_2) \tilde{g} \\ -(\tilde{x}_1 + \tilde{x}_2) f_X \end{bmatrix} = \begin{bmatrix} \tilde{X} f_y - d \\ -\tilde{X} f_X \end{bmatrix} \tag{39}$$

using the fact that (from the second line of (33))

$$\tilde{Q} g(\tilde{Q}) = d. \tag{40}$$

So to leading order the eigenvector corresponding to eigenvalue $\sqrt{\epsilon} bi + o(\sqrt{\epsilon})$ is

$$\mathbf{w_0} + \mathbf{w_e} = \begin{bmatrix} 1 \\ -1 - \sqrt{\epsilon} Bi \\ \sqrt{\epsilon} Ci \end{bmatrix} \quad \text{for some } B, C > 0. \tag{41}$$

Now we add total prey as a fourth state variable to the system. The corresponding eigenvector component is the sum of the first two components in (41) (see Appendix A):

$$\begin{bmatrix} 1 \\ -1 - \sqrt{\epsilon} Bi \\ \sqrt{\epsilon} Ci \\ -\sqrt{\epsilon} Bi \end{bmatrix} \tag{42}$$

We can multiply each component of (42) by an arbitrary real constant without affecting the phase angles, so we can consider instead $\left(1, -1 - \sqrt{\epsilon} Bi, i, -i\right)^T$. Then as

$\epsilon \to 0$ the vector giving the relative phases for prey 1, prey 2, predator, and total prey becomes

$$[1 \quad -1 \quad i \quad -i]^T . \tag{43}$$

The components of the limiting phase-angle vector (43) lie exactly on the coordinate axes. The two prey types (first and second eigenvector components) are exactly out of phase; the predator and total prey (third and fourth components) are exactly out of phase; and there is a quarter-period lag between the vulnerable prey and the predator. This holds in the limit $\theta_1 \to \theta_2$ for $p_1 < p^*$ such that the coexistence equilibrium remains is an unstable spiral when $\theta_1 < \theta_2$.

The occurrence of cryptic cycles (Fig. 1b) is explained by the asymptotic eigenvector (42) and the fact that $\tilde{x}_1, \tilde{x}_2$ converge to positive limits while $\tilde{y} \to 0$. Together they imply that the coefficient of variation in density over a complete cycle drops to zero for total prey, while remaining bounded above zero for the two prey types individually and increasing for the predator. The long period of evolutionary and cryptic cycles is explained by the zero eigenvalue for (35). The dominant eigenvalues for the coexistence equilibrium are a complex–conjugate pair (because of property 2 above) which converge on a double-zero root as $\theta_1 \uparrow \theta_2$. The cycle period near the equilibrium is inversely proportional to the imaginary part of the dominant eigenvalues. As $\theta_1 \uparrow \theta_2$, the imaginary part of the dominant eigenvalues remains positive but becomes increasingly small, so cycles near the equilibrium have longer and longer period that increases without limit as $\theta_1 \uparrow \theta_2$. See [48] for further details and data analyses supporting these predictions.

7 Discussion

The model studied in this paper is three dimensional, with a few fairly tame nonlinearities—just like the Lorenz equations. So it is not surprising that a complete mathematical analysis of it has not been possible. Nonetheless, we have come a long way towards our goal of characterizing how and when rapid evolution can affect the ecological dynamics resulting from predator–prey interactions.

Our primary questions concern the generality of the phenomenon of "evolutionary" limit cycles in predator–prey interactions, and the conditions in which such cycles might be observed. A combination of analysis and numerical studies suggests that evolutionary dynamics are not omnipresent, but neither are they knife-edge phenomena existing only in a narrow range of parameter values. Instead, the types of cycles observed by Yoshida et al. [46,48] are both robust and general. They occur in a specific but substantial and biologically relevant region of the parameter space, and in a general class of predator-two prey models that includes a two-prey model with Lotka–Volterra prey competition terms [1,2,26], and the standard two prey chemostat model [12,24,46] with mechanistic modeling of resource competition between the prey.

We have shown that evolutionary cycles arise through a bifurcation from a stable coexistence equilibrium, that occurs when defense against predation remains relatively inexpensive but nevertheless becomes very effective. Cryptic population dynamics,

where the predator cycles but the total prey density remains nearly constant, occur as a limiting case when effective defense comes at almost zero cost [48]. These regions in parameter space are biologically relevant because empirical studies have shown that defense—be it against predation or against antimicrobial compounds—can arise quickly and can be both highly effective and very cheap [3,17,47]. For example, Gagneux et al. [17] showed that in laboratory cultures of *Mycobacterium tuberculosis* (TB) mutants, prolonged treatment with antibiotics results in multi-drug resistant strains of TB with no fitness costs for resistance, and furthermore that most naturally circulating resistant TB strains are either low or no cost types. Indeed, fitness tradeoffs in the production of defensive structures and compounds are notoriously difficult to demonstrate, and in many empirical studies, no fitness tradeoff was actually found [3,9,41].

We close by listing some open questions. "Proving things is hard" (H. Smith, personal communication), but others may succeed where we have not. Concerning the model in this paper,

- When does the Jacobian at a coexistence equilibrium have a pair of complex conjugate eigenvalues? There will be 3 real, negative eigenvalues if the two prey types are very similar and the interior equilibrium for the (predator + vulnerable prey) exists and is a stable node. However, our numerical results suggest the full system (at a coexistence equilibrium) has complex conjugate eigenvalues whenever the (predator+vulnerable prey) system has an interior equilibrium with complex conjugate eigenvalues.
- Can there be coexistence of the predator and both prey on a limit cycle or other attractor, even when there is no coexistence equilibrium? Numerical evidence suggests that the answer is "no" for the chemostat model: for k_1 below (above) the range of values at which a coexistence equilibrium exists, the defended (vulnerable) prey type outcompetes the other. As it is difficult to distinguish between persistence and slow competitive exclusion numerically, it is likewise hard to map reliably the parameter region where both prey coexist on a nonpoint attractor.
- On the bifurcation curve $0 \le p_1 \le p^*,\ k_1 = k_2$, the Jacobian of the general model (33) has zero as a double root with algebraic multiplicity 2 and geometric multiplicity 1. Generically, this situation gives a *Takens–Bogdanov* bifurcation [27]. Do the higher order conditions for Takens–Bogdanov (i.e., BT.1–BT.3 in Theorem 8.4 of [27]), which hold generically, hold for our model (2)?
- A general two-prey, one-predator chemostat can exhibit a wider range of dynamic behaviors than we have observed in a system where the prey differ only in their p and k values (see [44] and references therein). Indeed, these predicted dynamics have been observed in other experimental systems [8]. The absence of some dynamics from our system could indicate a qualitative difference between within-species evolutionary dynamics resulting from prey genetic diversity, and food-web dynamics with one predator feeding on a several prey species whose within-species heritable variation is much smaller than the functional differences among prey species. But another possibility is that more complex dynamics can occur, at parameters outside the range we have explored.

More generally, how robust are the phenomena of evolutionary and cryptic predator–prey cycles in more complex food webs involving multiple predator and prey species?

Acknowledgments This research was supported by grants from the Andrew W. Mellon Foundation to SPE and Nelson G. Hairston Jr.. We thank the other members of the Cornell EEB rotifer–alga chemostat group (Rebecca Dore, Gregor Fussmann, Nelson Hairston Jr., Justin Meyer and Takehito Yoshida) for their support and many discussions on this project. For helpful comments on the manuscript we thank Alan Hastings, an anonymous referee, the Cornell Eco-Theory lunch–bunch, and especially Parviez Hosseini.

Appendices

Appendices A and B summarize some general results useful to us here, and contain nothing original. In Appendix C we derive the expressions for coexistence steady states in the reduced and rescaled two-prey chemostat model, and in Appendix D we derive the Jacobian matrix and prove that it has negative determinant at any coexistence steady state. In Appendix E we derive the conditions in which a limit cycle of the (predator + edible prey) subsystem can can be invaded by the defended prey. Finally, in Appendix F we show generally that for realized cost θ_1 sufficiently close to θ_2 and $0 \le p_1 \le p^*$, the coexistence equilibrium for the general model (33) always has a pair of complex conjugate eigenvalues.

A Appendix: Eigenvectors and phase relations

The contents of this Appendix appear to be well-known, but we have not seen them summarized anywhere in print. We consider oscillations in a linear system

$$\dot{x} = \mathbf{J}x \tag{44}$$

resulting from the real matrix $\mathbf{J}$ having complex conjugate eigenvalues

$$\lambda, \bar{\lambda} = a \pm ib \text{ with } b > 0,$$

where $i = \sqrt{-1}$ and the over bar denotes complex conjugation. The corresponding eigenvectors are also a complex conjugate pair w, $\bar{w}$.

The resulting oscillatory terms in solutions of (44) are of the general form $Ae^{\lambda t}w + Be^{\bar{\lambda}t}\bar{w}$. In order for these to be real (as solutions of (44) must be), we must have $B = \bar{A}$. Then writing $A = re^{i\theta}$, $r > 0$, the solutions are proportional to

$$z(t) \equiv e^{i\theta}e^{ibt}w + e^{-i\theta}e^{-ibt}\bar{w}. \tag{45}$$

We are interested in the relative phases of the oscillations by different components in $z(t)$. Write $w_j = r_j e^{i\phi_j}$ for the j^{th} component of w. The j^{th} component of $z(t)$ is then

$$r_j(e^{i(\phi_j+\theta+bt)} + e^{-i(\phi_j+\theta+bt)}) = 2r_j\cos(\phi_j + \theta + bt). \tag{46}$$

The relative phases of the j^{th} and k^{th} components in solutions proportional to $z(t)$ is therefore given by $\phi_j - \phi_k$. When this is near 0 components j and k are oscillating in phase, and when it is near $\pm\pi$ they are oscillating nearly out of phase.

We are interested in the phase difference between the predators and total prey density. For that we can use a linear change of variables

$$\begin{bmatrix} u \\ v \\ y \end{bmatrix} = \begin{bmatrix} x_1 + x_2 \\ x_1 - x_2 \\ y \end{bmatrix} = \mathbf{A} \begin{bmatrix} x_1 \\ x_2 \\ y \end{bmatrix}, \quad \mathbf{A} = \begin{bmatrix} 1 & 1 & 0 \\ 1 & -1 & 0 \\ 0 & 0 & 1 \end{bmatrix}.$$

In transformed coordinates the Jacobian matrix becomes $\mathbf{AJA}^{-1}$, and Jacobian eigenvectors w are transformed to $\mathbf{A}w$. The dominant eigenvector component for $x_1 + x_2$ is therefore the sum of the components for x_1 and x_2.

B Appendix: Stability conditions

In this Appendix we review criteria for local stability of equilibria in a three-dimensional system of ordinary differential equations.

The diagonal expansion ([39], Sect. 4.6) is an expression for $\det(A + D)$ where A is square and D is diagonal. For $D = xI$ and A of order n it states that

$$\det(A + xI) = x^n + x^{n-1}T_1(A) + x^{n-2}T_2(A) + \cdots + T_n(A) \tag{47}$$

where $T_j(A)$ is the sum of all principal minors of order j (a principal minor of order j is the determinant of a $j \times j$ submatrix of A whose diagonal is a subset of the diagonal of A—that is, a submatrix obtained by selecting $n - j$ diagonal elements of A and deleting the row and column containing each element). Note that $T_n(A) = \det(A)$ and $T_1(A) = \text{trace}(A)$.

For a 3×3 matrix the characteristic polynomial is

$$p(\lambda) \equiv \det(\lambda I - A) = \lambda^3 + c_2\lambda^2 + c_1\lambda + c_0. \tag{48}$$

Comparing with (47) and noting that and that $T_j(-A) = (-1)^j T_j(A)$, we have

$$\begin{aligned} c_0 = T_3(-A) = -\det(A), \quad c_1 = T_2(-A) = T_2(A), \\ c_2 = \text{trace}(-A) = -\text{trace}(A). \end{aligned} \tag{49}$$

In the notation of (48), the Routh–Hurwitz stability criteria for order-3 systems [28] is

$$c_0 > 0, \quad c_1 > 0, \quad c_2 > 0, \quad c_1c_2 > c_0. \tag{50}$$

Loss of stability through a Hopf bifurcation occurs when the third condition in (50) is violated, with the c_i all positive [19].

C Coexistence steady states for the rescaled chemostat model

We consider here the two-prey model (9). Setting $\dot{y} = 0$ and solving gives the steady state value of Q, $\tilde{Q} = \frac{k_b}{g-1}$. We solve for $\tilde{X}$ and $\tilde{y}$ as follows. Defining $Z = 1 - X - y$ and noting that $\frac{g}{k_b+\tilde{Q}} = \frac{1}{\tilde{Q}}$, the conditions $\dot{x}_1 = \dot{x}_2 = 0$ imply

$$\frac{m\tilde{Z}}{k_1 + \tilde{Z}} - \frac{p_1\tilde{y}}{\tilde{Q}} = \frac{m\tilde{Z}}{k_2 + \tilde{Z}} - \frac{\tilde{y}}{\tilde{Q}} = 1. \tag{51}$$

Solving (51) for $\tilde{y}$ gives two expressions which remain equal within the coexistence region:

$$\tilde{y} = \frac{\tilde{Q}}{p_1}\left[\frac{(m-1)\tilde{Z} - k_1}{k_1 + \tilde{Z}}\right], \quad \tilde{y} = \tilde{Q}\left[\frac{(m-1)\tilde{Z} - k_2}{k_2 + \tilde{Z}}\right]. \tag{52}$$

Setting the two expressions for $\tilde{y}$ equal, we can solve for $\tilde{Z}$:

$$\tilde{Z} = \frac{1}{2(1-p_1)(m-1)}\left[\zeta + \sqrt{\zeta^2 + 4(m-1)(1-p_1)^2 k_1 k_2}\right] \tag{53}$$

where

$$\zeta = k_1\left(1 + p_1(m-1)\right) - k_2\left((m-1) + p_1\right).$$

Finally, recalling that $\tilde{Z} = 1 - \tilde{X} - \tilde{y}$, then $\tilde{X} = 1 - \tilde{Z} - \tilde{y}$. Expressions for $\tilde{x_1}$ and $\tilde{x_2}$ in terms of $\tilde{X}$ and $\tilde{Q}$ are derived and shown in the text.

D Jacobian at a coexistence equilibrium

The general expression (11) for Jacobian entries at a coexistence equilibrium implies that all entries in the ith row of the Jacobian have common factor $\tilde{x}_i$, so $\det(J) = \tilde{x}_1\tilde{x}_2\tilde{y}\det(\tilde{J})$ where $\tilde{J}(i,j) = \frac{\partial \tilde{r}_i}{\partial x_j}$ with $x_3 = y$. Let $\tilde{F}$ denote the steady state per-capita feeding rate for the predator,

$$\tilde{F} = \frac{1}{k_b + p_1\tilde{x}_1 + p_2\tilde{x}_2}, \tag{54}$$

and the a_i are defined by (31) with $\tilde{Z} = 1 - \tilde{x}_1 - \tilde{x}_2 - \tilde{y}$; Eq. (53) gives the general expression for $\tilde{Z}$.

Taking the necessary partial derivatives for model (9) we have:

$$\tilde{J} = \begin{bmatrix} -a_1 + gp_1^2\tilde{y}\tilde{F}^2 & -a_1 + gp_1p_2\tilde{y}\tilde{F}^2 & -a_1 - gp_1\tilde{F} \\ -a_2 + gp_1p_2\tilde{y}\tilde{F}^2 & -a_2 + gp_2^2\tilde{y}\tilde{F}^2 & -a_2 - gp_2\tilde{F} \\ p_1gk_b\tilde{F}^2 & p_2gk_b\tilde{F}^2 & 0 \end{bmatrix}. \tag{55}$$

We now show that the determinant of the Jacobian is always negative for the general model (33), and therefore for the chemostat model, unless $p_1 = p_2$. For (33) with the scaling $p_2 = 1$ we have

$$\tilde{J} = \begin{bmatrix} f_X - p_1^2\tilde{y}\tilde{g}' & f_X - p_1\tilde{y}\tilde{g}' & f_y - p_1\tilde{g} \\ f_X - p_1\tilde{y}\tilde{g}' & f_X - \tilde{y}\tilde{g}' & f_y - \tilde{g} \\ \tilde{h}'p & \tilde{h}' & 0 \end{bmatrix} \tag{56}$$

where $\tilde{g} = g(\tilde{Q})$, $\tilde{g}' = g'(\tilde{Q})$ and $\tilde{h}' = h'(\tilde{Q})$, $h(Q) = Qg(Q)$. Then using basic products of determinants, $\det(\tilde{J})$ equals

$$\tilde{h}' \begin{vmatrix} f_X & f_X & f_y - p_1\tilde{g} \\ f_X & f_X & f_y - p_1\tilde{g} \\ p_1 & 1 & 0 \end{vmatrix} = \tilde{h}' \begin{vmatrix} f_X & f_X & f_y - p_1\tilde{g} \\ 0 & 0 & (p_1 - 1)\tilde{g} \\ p_1 & 1 & 0 \end{vmatrix} = (1 - p_1)^2\tilde{h}'\tilde{g}f_X \tag{57}$$

which is negative (unless $p_1 = 1$) because $\tilde{h}' > 0$, $\tilde{g} > 0$ and $f_X < 0$.

E Appendix: Invasion of an edible prey limit cycle

Following [2] we give here the condition for invasion of a predator + edible prey limit cycle by a rare defended prey type. Along the limit cycle we have $\langle \dot{\log y} \rangle = 0$ and therefore $\left\langle \frac{gx_2}{k_b + x_2} \right\rangle = 1$. By Jensen's inequality, this implies that $\frac{g\langle x_2 \rangle}{k_b + \langle x_2 \rangle} > 1$, and therefore $\langle x_2 \rangle > \tilde{Q}$. We also have $\langle \dot{\log x_2} \rangle = 0$ along the limit cycle, so

$$\left\langle \frac{gy}{k_b + x_2} \right\rangle = 1 + \left\langle \frac{m(1 - x_2 - y)}{k_2 + 1 - x_2 - y} \right\rangle. \tag{58}$$

A rare defended prey can invade if $\langle \dot{\log x_1} \rangle > 0$, i.e., if

$$0 < \left\langle \frac{m(1 - x_2 - y)}{k_1 + 1 - x_2 - y} - p_1 \frac{gy}{k_b + x_2} - 1 \right\rangle = \left\langle \frac{m(1 - x_2 - y)}{k_1 + 1 - x_2 - y} \right\rangle - p_1 \left\langle \frac{gy}{k_b + x_2} \right\rangle - 1$$

Using (58) and simplifying, we get the invasion condition in terms of p_1, k_1):

$$p_1 < \frac{\langle \zeta(k_1) \rangle - 1}{\langle \zeta(k_2) \rangle + 1}, \tag{59}$$

where

$$\zeta(k_i) = \frac{m(1 - x_2 - y)}{k_i + 1 - x_2 - y}.$$

Note that the right-hand side of (59) can be computed for all k_1 using one long simulation of the (predator + vulnerable prey) system, and yields p_1 as a function of k_1.

F Appendix: Eigenvalues for $\theta_1 \uparrow \theta_2$, $p_1 \leq p^*$

We show here that for θ_1 sufficiently close to θ_2 and $0 \leq p_1 \leq p^*$ in the general model (33), the coexistence equilibrium always has a pair of complex conjugate eigenvalues. As $\theta_1 \to \theta_2$, in this range of p_1 values $\tilde{y} \to 0$, so we set $\tilde{y} = \epsilon \ll 1$ and use a series expansion in ϵ of the characteristic polynomial (i.e., we regard θ_1 as a function of $\tilde{y}$ with all else held fixed, rather than *vice versa*). The Jacobian at the coexistence equilibrium is an $O(\epsilon)$ perturbation of (35) and so to leading order has the form

$$J(\epsilon) = \begin{bmatrix} A + \epsilon a_{11} & A + \epsilon a_{12} & B + \epsilon a_{13} \\ C + \epsilon a_{21} & C + \epsilon a_{22} & D + \epsilon a_{23} \\ \epsilon a_{31} & \epsilon a_{32} & 0 \end{bmatrix} \tag{60}$$

with $A, B, C, D < 0$, and $a_{31} = p_1 a_{32} > 0$ (the last holds because $\dot{y}/y$ is a function of $Q = p_1 x_1 + x_2$ with the scaling $p_2 = 1$). $J(0)$ has eigenvalues zero (with algebraic multiplicity 2) and $A + C < 0$, and we need to approximate the near-zero eigenvalues for ϵ small. The characteristic polynomial of $J(\epsilon)$ is a cubic in λ but the near-zero eigenvalues are at most $O(\sqrt{\epsilon})$, so for our purpose the λ^3 terms in the characteristic polynomial can be neglected. This leaves a quadratic polynomial in λ, which will have complex conjugate roots if its discriminant is negative. Using Maple to compute the characteristic polynomial of (60), discard λ^3 terms and expand the remainder about $\epsilon = 0$, to leading order in ϵ the discriminant is

$$4\epsilon(a_{32} - a_{31})(A + C)(AD - BC)$$

which will be negative if $AD - BC > 0$. Referring to (35) some algebra gives

$$AD - BC = \tilde{x}_1 \tilde{x}_2 \tilde{f}_X \tilde{g}(p_1 - 1)$$

which is positive because $f_X < 0$, as desired.

References

1. Abrams, P., Matsuda, H.: Prey adaptation as a cause of predator–prey cycles. Evolution **51**, 1742–1750 (1997)
2. Abrams, P.: Is predator-mediated coexistence possible in unstable systems? Ecology **80**, 608–621 (1999)
3. Andersson, D.I., Levin, B.R.: The biological cost of antibiotic resistance. Curr. Opin. Microbiol. **2**, 489–493 (1999)
4. Antonovics, J., Bradshaw, A.D., Turner, R.G.: Heavy metal tolerance in plants. Adv. Ecol. Res. **71**, 1–85 (1971)
5. Arino, J., Pilyugin, S., Wolkowicz, G.S.K.: Considerations on yield, nutrient uptake, cellular growth, and competition in chemostat models. Can. Appl. Math. Quart. **11**, 107–142 (2003)
6. Ashley, M.V., Willson, M.F., Pergams, O.R.W., O'Dowd, D.J., Gende, S.M., Brown, J.S.: Evolutionarily enlightened management. Biol. Conserv. **111**, 115–123 (2003)
7. Barry, M.: The costs of crest induction for Daphnia carinata. Oecologia **97**, 278–288 (1994)
8. Becks, L., Hilker, F.M., Malchow, H., Jürgens, K., Arndt, H.: Experimental demonstration of chaos in a microbial foodweb. Nature **435**, 1226–1229 (2005)

9. Bergelson, J., Purrington, C.B.: Surveying patterns in the cost of resistance in plants. Am. Nat. **148**, 536–558 (1996)
10. Bohannan, B.J.M., Lenski, R.: Effect of resource enrichment on a chemostat community of bacteria and bacteriophage. Ecology **78**, 2303–2315 (1997)
11. Bohannan, B.J.M., Lenski, R.: Effect of prey heterogeneity on the response of a model food chain to resource enrichment. Am. Nat. **153**, 73–82 (1999)
12. Butler, G.J., Wolkowicz, G.S.K.: Predator-mediated competition in the chemostat. J. Math. Biol. **24**, 167–191 (1986)
13. Coltman, D.W., O'Donoghue, P., Jorgenson , J.T., Hogg, J.T., Strobeck, C., Festa-Blanchet, M.: Undesirable evolutionary consequences of trophy-hunting. Nature **426**, 655–658 (2003)
14. Conover, D.O., Munch, S.B.: Sustaining fisheries yields over evolutionary time scales. Science **297**, 94–96 (2002)
15. Fussmann, G.F., Ellner, S.P., Shertzer, K.W., Hairston, N.G. Jr.: Crossing the Hopf bifurcation in a live predator–prey system. Science **290**, 1358–1360 (2000)
16. Fussmann, G.F., Ellner, S.P., Hairston, N.G. Jr.: Evolution as a critical component of plankton dynamics. Proc. Roy. Soc. Lond. Ser B **270**, 1015–1022 (2003)
17. Gagneux, S., Long, C.D., Small, P.M., Van, T., Schoolnik, G.K., Bohannan, B.J.M.: The competitive cost of antibiotic resistance in *Mycobacterium tuberculosis*. Science **312**, 1944–1946 (2006)
18. Grant, P.R., Grant, B.R.: Unpredictable evolution in a thirty year study of Darwin's finches. Science **296**, 707–710 (2002)
19. Guckenheimer, J., Myers, M., Sturmfels, B.: Computing Hopf bifurcations I. SIAM J. Numer. Anal. **34**, 1–27 (1997)
20. Hairston, N.G., Walton, W.E.: Rapid evolution of a life-history trait. Proc. Natl. Acad. Sci. USA **83**, 4831–4833 (1986)
21. Hairston, N.G., Ellner, S.P., Geber, M.A., Yoshida, T., Fox, J.A.: Rapid evolution and the convergence of ecological and evolutionary time. Ecol. Lett. **8**, 1114–1127 (2005)
22. Heath, D.D., Heath, J.W., Bryden, C.A., Johnson, R.M., Fox, C.W.: Rapid evolution of egg size in captive salmon. Science **299**, 1738–1740 (2003)
23. Hendry, A.P., Kinnison, M.T.: The pace of modern life: measuring rates of contemporary microevolution. Evolution **53**, 1637–1653 (1999)
24. Jones, L.E., Ellner, S.P.: Evolutionary tradeoff and equilibrium in a predator–prey system. Bull. Math. Biol. **66**, 1547–1573 (2004)
25. Kinnison, M.T., Hairston, N.G. Jr.: Eco-evolutionary conservation biology: contemporary evolution and the dynamics of persistence. Funct. Ecol. (submitted) (2006)
26. Kretzschmar, M., Nisbet, R.M., McCauley, E.: A predator–prey model for zooplankton grazing on competing algal populations. Theor. Pop. Biol. **44**, 32–66 (1993)
27. Kuznetsov, Y.A.: Elements of applied bifurcation theory. Applied Mathematical Sciences, vol. 112, Chap. 8. Springer, New York (1994)
28. May, R.M.: Stability and complexity in model ecosystems. Princeton University Press, Princeton, New York (1974)
29. Meyer, J., Ellner, S.P., Hairston, N.G. Jr., Jones, L.E., Yoshida, T.: Prey evolution of the time scale of predator–prey dynamics revealed by allele-specific quantitative PCR. Proc. Natl. Acad. Sci. **103**, 10690–10695 (2006)
30. Olsen, E.M., Heino, M., Lilly, G.R., Morgan, M.J., Brattey, J., Dieckmann, U.: Maturation trends indicative of rapid evolution preceded the collapse of northern cod. Nature **428**, 932–935 (2004)
31. Palumbi, S.: The evolution explosion: how humans cause rapid evolutionary change. Norton W.W., New York (2001)
32. Pickett-Heaps, J.D.: Green Algae: Structure, Reproduction and Evolution in Selected Genera. Sinauer Associates, Sunderland (1975)
33. Press, W.H., Flannery, B.P., Teukolsky, S.A., Vetterling, W.T.: Numerical Recipes in C. Cambridge University Press, Cambridge (1988)
34. Preisser, E.L., Bolnick, D.J., Benard, M.F.: Scared to Death? The effects of intimidation and consumption in predator–prey interactions. Ecology **86**, 501–509 (2005)
35. Reznick, D.N., Shaw, F.H., Rodd, F.H., Shaw, R.G.: Evaluation of the rate of evolution in natural populations of guppies (*Poecilia reticulata*). Science **275**, 1934–1937 (1997)
36. Ruan, S., Wolkowicz, G.S.K.: Bifurcation of a chemostat model with a distributed delay. J. Math. Anal. Appl. **204**, 786–812 (1996)

37. Saccheri, I., Hanski, I.: Natural selection and population dynamics. Trends Ecol. Evolut. **21**, 341–347 (2006)
38. Shertzer, K.W., Ellner, S.P., Fussmann, G.F., Hairston, N.G. Jr.: Predator–prey cycles in an aquatic microcosm: testing hypotheses of mechanism. J. Anim. Ecol. **71**, 802–815 (2002)
39. Searle, S.R.: Matrix Algebra Useful for Statistics. Wiley, New York (1982)
40. Smith, H.L., Waltman, P.: The Theory of the Chemostat. Cambridge University Press, Cambridge (1995)
41. Strauss, S.Y., Rudgers, J.A., Lau, J.A., Irwin, R.E.: Direct and ecological costs of resistance to herbivory. Trends Ecol. Evol. **17**, 278–285 (2002)
42. Thompson, J.N.: Rapid evolution as an ecological process. Trends Ecol. Evol. **13**, 329–332 (1998)
43. Toth, D., Kot, M.: Limit cycles in a chemostat model for a single species with age structure. Math. Biosci. **202**, 194–217 (2006)
44. Vayenis, D.V., Pavlou, S.: Chaotic dynamics of a food web in a chemostat. Math. Biosci. **162**, 69–84 (1999)
45. Xia, H., Wolkowicz, G.S.K., Wang, L.: Transient oscillation induced by delayed growth response in the chemostat. J. Math. Biol. **50**, 489–530 (2005)
46. Yoshida, T., Jones, L.E., Ellner, S.P., Fussmann, G.F., Hairston, N.G. Jr.: Rapid evolution drives ecological dynamics in a predator–prey system. Nature **424**, 303–306 (2003)
47. Yoshida, T., Ellner, S.P., Hairston, N.G. Jr.: Evolutionary tradeoff between defense against grazing and competitive ability in a simple unicellular alga, *Chlorella vulgaris*. Proc. Roy. Soc. Lond. B. **271**, 1947–1953 (2004)
48. Yoshida, T., Ellner, S.P., Jones, L.E., Hairston, N.G. Jr.: Cryptic population dynamics: rapid evolution masks trophic interaction. PLOS Biol. (submitted) (2007)
49. Zimmer, C.: Rapid evolution can foil even the best-laid plans. Science **300**, 895 (2003)